Predicting polycyclic aromatic hydrocarbon formation with an automatically generated mechanism for acetylene pyrolysis

Predicting polycyclic aromatic hydrocarbon formation with an automatically generated mechanism for acetylene pyrolysis

Mengjie Liu[a], Te-Chun Chu[a], Agnes Jocher[a], Mica C. Smith[a], Istvan Lengyel[b], William H. Green[a,*]

[a]*Department of Chemical Engineering, Massachusetts Institute of Technology, Cambridge, MA 02139, United States*
[b]*SABIC Technology Center, 1600 Industrial Boulevard, Sugar Land, TX 77478, United States*

Abstract

Using Reaction Mechanism Generator (RMG), we have automatically constructed a detailed mechanism for acetylene pyrolysis which predicts formation of polycyclic aromatic hydrocarbons up to pyrene. To improve the data available for formation pathways from naphthalene to pyrene, new high-pressure limit reaction rate coefficients and species thermochemistry were calculated using a combination of electronic structure data from literature and new quantum calculations. Pressure-dependent kinetics for the C_4H_4 potential energy surface calculated by Zádor *et al.* [J. Phys. Chem. A 2017; 121(22)] were incorporated to ensure accurate pathways for acetylene initiation reactions. After adding these new data into the RMG-database, a pressure-dependent mechanism was generated in a single RMG simulation which captures chemistry from C_2 to C_{16}. In general, the RMG-generated model accurately predicts major species profiles in comparison to plug-flow reactor data from literature. The primary short-coming of the model is that formation of anthracene, phenanthrene, and pyrene are underpredicted, and PAHs beyond pyrene are not captured. Reaction path analysis was performed for the RMG model to identify key pathways. Notable conclusions include the importance of accounting for the acetone impurity in acetylene in accurately predicting formation of odd-carbon species, the remarkably low contribution of acetylene dimerization to vinylacetylene or diacetylene, and the dominance of the HACA mechanism in the formation pathways to all PAH species in the model. This work demonstrates the improved ability of RMG to model PAH formation, while highlighting the need for more kinetics data for elementary reaction pathways to larger PAHs.

Keywords: Reaction Mechanism Generator, polycyclic aromatic hydrocarbon, acetylene, pyrolysis, detailed mechanism

1. Introduction

Polycyclic aromatic hydrocarbon (PAH) formation occurs in a wide range of systems, from combustion and pyrolysis of conventional fuels[1] to carbon-rich circumstellar envelopes.[2, 3] PAHs are known to be harmful to human health [4] and are also precursors to soot, which lead to additional health and environmental hazards.[1, 5] There has been ongoing interest in understanding the chemical mechanisms involved

*Corresponding author
Email address: whgreen@mit.edu (William H. Green)

in PAH formation for many decades, yet there is still much which is unclear.

Numerous PAH formation pathways have been proposed and studied to date. Broadly speaking, possible routes to forming the first aromatic ring (*i.e.*, benzene) include C_2 + C_4 pathways,[6, 7, 8], C_3 + C_3 pathways,[9, 10] and C_5 + C pathways.[11, 12, 13] Even more pathways have been studied for formation of the second aromatic ring (*i.e.*, indene and naphthalene), most of which were summarized thoroughly by Mebel *et al.*[14] Many pathways to forming the second ring are also extensible to formation of larger PAHs. Most notable is the well-known hydrogen abstraction, C_2H_2 addition (HACA) pathway, which was proposed by Frenklach *et al.*,[6] and a closely related route proposed by Bittner and Howard.[15] HACA pathways have been studied starting from phenyl,[16] naphthalenyl,[17, 18, 19] biphenylyl,[20] and phenanthryl.[21] Vinylacetylene addition also provides a route to adding another aromatic ring, which has been calculated for phenyl [22] and naphthalenyl.[23] Finally, addition of phenyl [24, 25, 26] and benzyne [26, 27] have also been studied as a direct pathway to an additional aromatic ring.

Furthermore, the initiation mechanism for acetylene pyrolysis is of interest. There has been much discussion regarding the relative importance of radical initiation pathways (e.g. addition and H-loss to C_4H_3 or disproportionation to C_2H_3 and C_2H) or isomerization to vinylidene.[28, 29, 30] It is possible that acetone impurities which are typically present in acetylene may contribute to initiation,[31] although there has also been work suggesting that there is negligible effect.[32] More recently, there have been a few computational studies of acetylene initiation steps,[33, 34, 35] and in particular, Zádor *et al.* concluded that vinylidene formation followed by addition to acetylene is the primary initiation pathway.

There have been a number of previously published mechanisms specifically for acetylene pyrolysis including PAH formation, including early work by Frenklach *et al.*,[6] and more recent ones by Norinaga *et al.*,[36] Slavinskaya *et al.*,[37] and Tao *et al.*[38] Norinaga *et al.* compiled elementary reactions reported in literature to obtain a mechanism predicting up to the formation of coronene. They included acetone in their model to be consistent with their experiments, which used acetylene feed containing acetone and methane impurities. Slavinskaya *et al.* focused on optimizing model parameters to match numerous experimental data in the literature, focusing on C_1-C_4 chemistry, with the final mechanism including species up to benzo[a]pyrene. Tao *et al.* combined previously published acetylene mechanisms to construct an improved mechanism for predicting the formation of 7 U.S. Environmental Protection Agency targeted PAHs up to coronene.

Developing detailed kinetic models for PAH formation is challenging because the variety of products and inclination to form soot make experimental investigations difficult, the size of PAHs make accurate quantum calculations difficult, and the number of species and reactions involved can make the mechanism generation process itself difficult. Automatic mechanism generation provides a useful tool to aid the latter by keeping track of all of the species and reactions, and automatically identifying ones which are relevant to the system of interest. Additionally, parameter estimation methods (*e.g.*, thermochemical group additivity and kinetics rate rules) enable straightforward prediction of unknown parameters. One such software is the Reaction Mechanism Generator (RMG), an open-source mechanism generation package written in Python.[39]

Previously, we have described efforts towards expanding the RMG-database with the necessary pathways and data to predict formation of one- and two-ring aromatic species.[40] Those efforts included the addition of new kinetics families for propargyl recombination and rate calculations for pathways forming naphthalene and acenaphthylene, which were combined to generate a pressure-dependent mechanism for methane oxidation using RMG. In this work, we focus on further improving the RMG database with key thermochemical and rate parameters for modeling PAH formation in acetylene pyrolysis. While the focus of these additions was on PAH formation pathways, initiation reactions for acetylene pyrolysis were also considered.

2. Methods

2.1. Kinetics libraries

High-pressure-limit rate coefficients have been calculated for a number of PAH formation pathways. In some cases, electronic structure results were obtained from literature, and in others, electronic structure calculations were performed using Gaussian 16 [41] (for CBS-QB3 and B3LYP calculations) and Molpro [42] (for CCSD(T) calculations). Rate coefficients were calculated using Arkane, a TST and master equation solver packaged with RMG.[43] Table 1 summarizes the reaction pathways for which rate coefficients were calculated.

Table 1: Potential energy surfaces (PES) for which high-pressure limit rate constants were calculated using Arkane. Reference column refers to source of electronic structure data.

PES	Reactants	Level of Theory	Reference
$C_{12}H_{11}$	phenyl + benzene	CBS-QB3	this work
$C_{12}H_{10}$	benzyne + benzene	CBS-QB3	this work
$C_{12}H_9$	naphthalenyl + acetylene	G3(MP2,CC)//B3LYP/6-311G(d,p)	this work
$C_{14}H_{11}$	vinylnaphthalenyl + acetylene	G3(MP2,CC)//B3LYP/6-311G(d,p)	this work
$C_{14}H_{11}$	naphthalenyl + vinylacetylene	G3(MP2,CC)//B3LYP/6-311G(d,p)	[23]
$C_{14}H_{11}$	biphenylyl + acetylene	G3(MP2,CC)//B3LYP/6-311G(d,p)	[20]
$C_{16}H_{11}$	phenanthracenyl + acetylene	G3(MP2,CC)//B3LYP/6-311G(d,p)	[21]

The phenyl + benzene and benzyne + benzene surfaces have been previously reported by Comandini *et al.* at the uCCSD(T)/cc-pVDZ//uB3LYP/6-311+G(d,p) level of theory.[27] Here, we recalculated the addition and H-loss reactions using CBS-QB3 to obtain more accurate energies.

The two surfaces for first and second addition of acetylene to naphthalenyl have been previously reported by Kislov *et al.*[17] and Frenklach *et al.*[18] For the $C_{14}H_{11}$ surface, 1D hindered-rotor scans were performed, and for the $C_{12}H_9$ surface, hindered-rotor scans were obtained from Frenklach *et al.*

The naphthalenyl + vinylacetylene surface was explored by Zhao *et al.*,[23] which provides a pathway to three aromatic rings requiring only a single addition reaction followed by ring-closing. The HACA pathways for closing the bay sites in biphenyl and phenanthracenyl via a single acetylene addition step were calculated by Yang *et al.* and Zhao *et al.*, respectively.[20, 21] For these surfaces, we used the published quantum results directly for rate coefficient calculations.

A kinetics library was also created for reactions on the $C_{14}H_9$ surface (*i.e.*, ethynylnaphthalenyl + acetylene) with high-pressure limit rate coefficients reported by Liu *et al.*[19] They performed calculations at the B3LYP//6-311+G(d,p) level of theory, and applied a correction calculated from the difference between CBS-QB3 and B3LYP//6-311+G(d,p) energies for the analogous benzene system.

To accurately capture acetylene initiation reactions, a kinetics library was created with reactions on the C_4H_4 potential energy surface using pressure-dependent rate coefficients calculated by Zádor *et al.*[35] Their calculations were performed at the CCSD(T)-F12b/cc-pVQZ-F12//M06-2X/MG3S level of theory, and master equation calculations were done using MESS.[44]

2.2. Thermochemistry libraries

Separate from the rate calculations, thermochemistry calculations were performed for all species from the PAH formation pathways which have been added to the RMG database. The calculated thermochemistry data can be found in CHEMKIN format in the supporting information. Electronic structure calculations using CBS-QB3 were performed using Gaussian 09 [45] and Gaussian 16, including 1D hindered-rotor calculations using B3LYP/CBSB7. Hindered rotor scans were performed automatically using ARC (Automatic Rate Calculator), a new Python package developed in our group for automating quantum chemistry calculations.[46] Thermochemistry calculations were also performed automatically by ARC using Arkane, with bond-additivity corrections from Petersson *et al.*[47]

2.3. Model generation

RMG v2.4.1 [48] was used to generate the acetylene pyrolysis model. An initial molar composition of 98% acetylene, 1.8% acetone, and 0.2% methane was used, based on the composition reported by Norinaga *et al.*[36] Reactor conditions were set with a temperature range of 1000-1500 K and a pressure of 0.2 atm. The pressure dependence feature of RMG was enabled, so that pressure dependent networks would be automatically constructed for species with up to 16 heavy atoms. Species constraints were set, limiting the maximum number of carbon atoms in any molecule to 20, and the maximum number of radicals to 1.

The kinetics library for the C_4H_4 surface was included as a seed mechanism. The other kinetics libraries containing high-pressure limit reaction rates for PAH formation pathways were combined into an aromatic sub-mechanism and appended to the final acetylene mechanism. In post-processing, a few highly-strained polycyclic species which were identified as being unreasonable were manually removed from the model. In general, these species were mistakenly identified by RMG as being important due to inaccurate thermochemistry estimation. In the end, the final model contains 1594 species and 8924 reactions. The model is

provided in CHEMKIN format with an RMG species dictionary in the supporting information. The aromatic sub-mechanism is also provided independently.

2.4. Model simulation and analysis

In this work, we chose to validate the model predictions using data from Norinaga *et al.* for acetylene pyrolysis in a flow reactor.[49] The primary reason for this choice was that they reported mole fractions of both small molecules and PAH species up to coronene as well as measured temperature profiles for their reactor.

Reactor simulations were performed using Cantera.[50] To simplify the simulation, we modeled a single fluid element flowing through the reactor as a homogeneous batch reactor. The residence time was dynamically calculated as a function of the reactor geometry and fluid density at a given position in the reactor and the mass flow rate. The mass flow rate was calculated assuming ideal gas, based on the fact that Norinaga *et al.* adjusted the flow rate to achieve 0.5s residence time in the isothermal region at each nominal temperature set point, neglecting composition effects.[49] The fluid density was obtained using Cantera functions, accounting for both temperature and composition. Temperature profiles and reactor geometry were obtained from Norinaga *et al.*[49]

While this approach tries to estimate the true residence time to the best of our ability, we note that there is still some uncertainty due to the assumptions made. We explored the effect of residence time uncertainty on the model predictions by performing isothermal simulations at residence times of 0.5s and 2s, which are shown in Figures S1-S3 in the supporting information.

Rate-of-production (ROP) analyses for the 1073 K and 1373 K set points also were performed with Cantera, using the same reactor simulation code. Sensitivity analysis was performed at 1373 K using RMG, which uses a constant temperature and pressure batch reactor.

3. Results and discussion

The RMG model predictions are shown in Figures 1–3, in comparison with the experimental measurements of Norinaga *et al.*[49] and predictions from published mechanisms by Norinaga *et al.*,[36] Slavinskaya *et al.*,[37] and Tao *et al.*[38] It is important to note that while the RMG and Norinaga mechanisms include acetone and related reactions, neither the Slavinskaya mechanism nor the Tao mechanism include acetone. As a result, the initial composition described by Norinaga *et al.*[36] including methane and acetone was used for simulations with the RMG and Norinaga mechanisms, while pure acetylene was used as the initial composition for simulations with the Slavinskaya and Tao mechanisms. The RMG mechanism was also simulated using pure acetylene for comparison. By comparing the two RMG simulations, we see that inclusion of acetone significantly affects both acetylene conversion and product distributions. These differences will be discussed in more detail shortly.

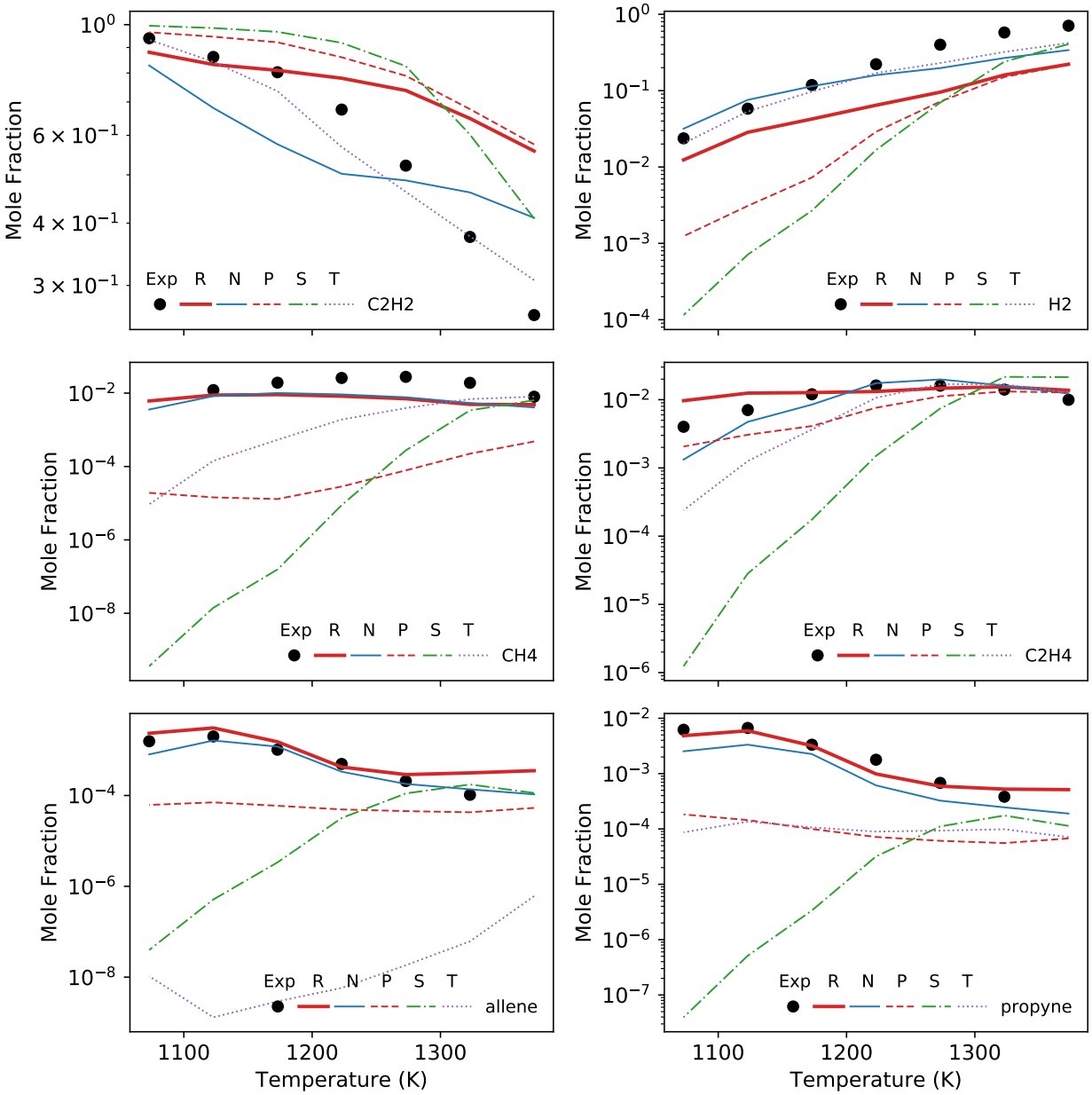

Figure 1: Final mole fractions as a function of nominal reactor temperature. Points are the experimental data from ref. [49], lines are the RMG model (R), Norinaga model (N), RMG model with pure acetylene (P), Slavinskaya model (S), and Tao model (T). Dashed lines are model simulations where the initial composition is pure acetylene.

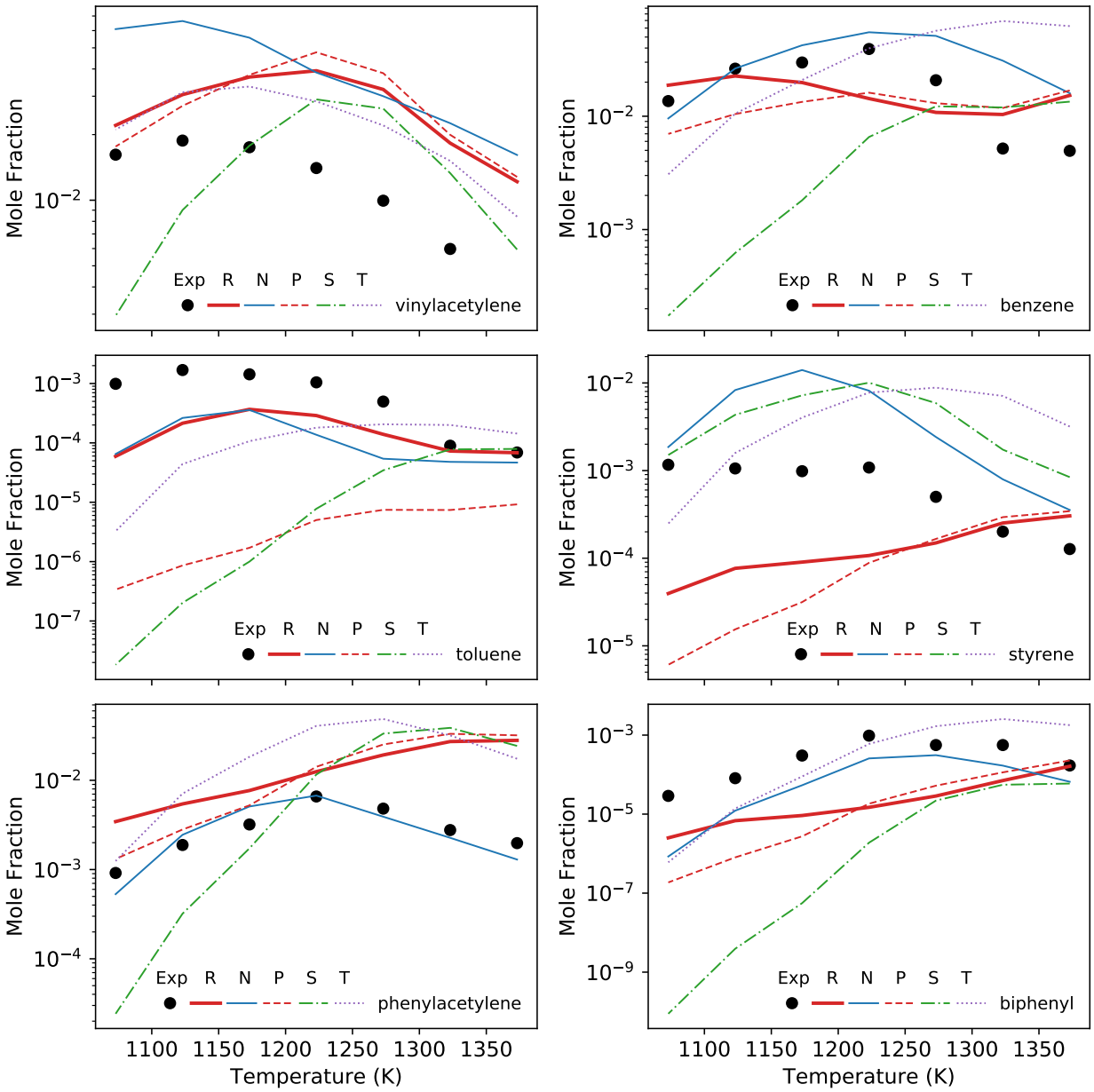

Figure 2: Final mole fractions as a function of nominal reactor temperature. Points are the experimental data from ref. [49], lines are the RMG model (R), Norinaga model (N), RMG model with pure acetylene (P), Slavinskaya model (S), and Tao model (T). Dashed lines are model simulations where the initial composition is pure acetylene.

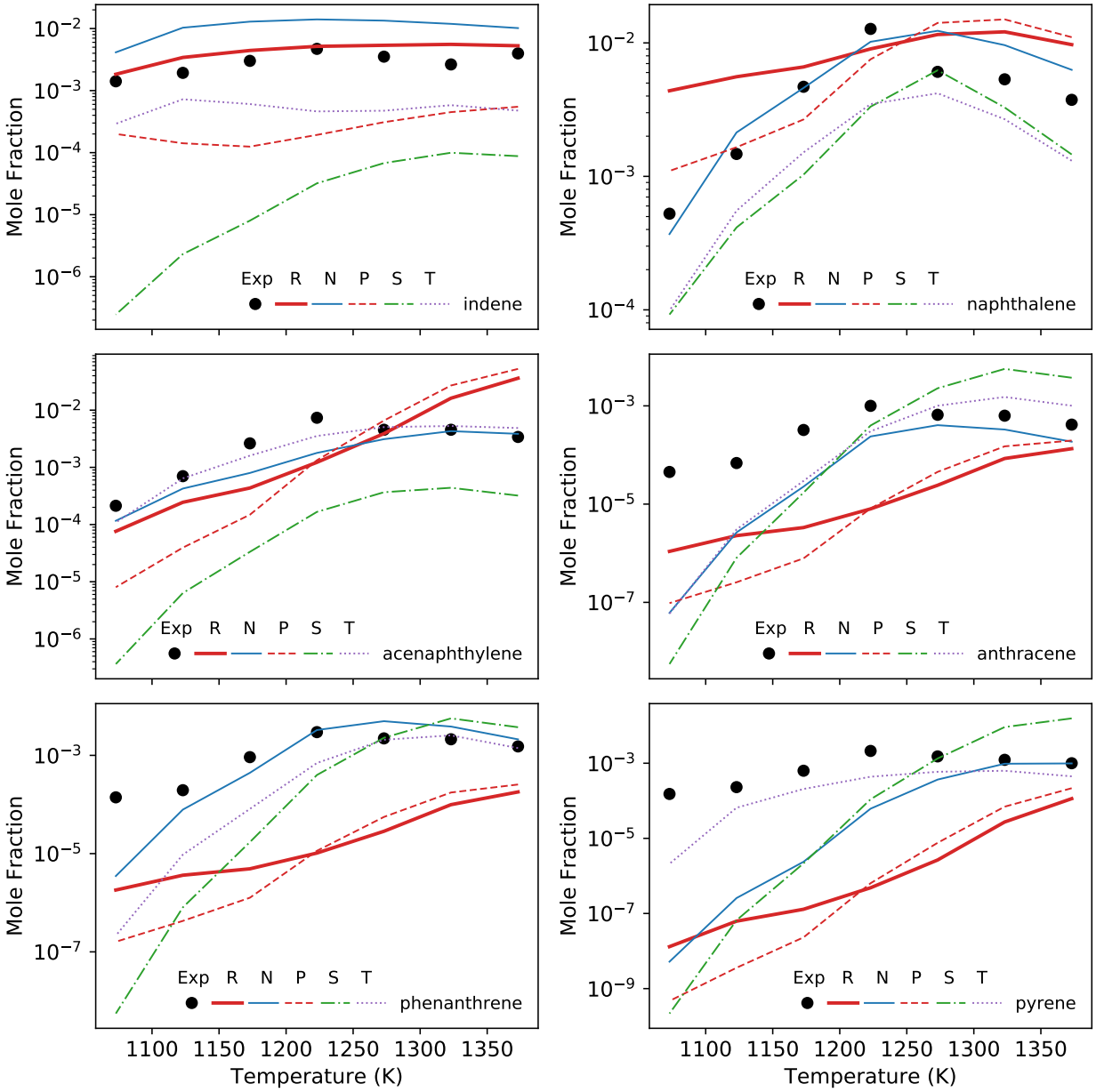

Figure 3: Final mole fractions as a function of nominal reactor temperature. Points are the experimental data from ref. [49], lines are the RMG model (R), Norinaga model (N), RMG model with pure acetylene (P), Slavinskaya model (S), and Tao model (T). Dashed lines are model simulations neglecting impurities in the acetylene feed.

3.1. Acetylene consumption

In Figure 1, we see that at higher temperatures, the RMG model predicts larger final mole fractions of acetylene than was observed in the experiment, *i.e.* less conversion of acetylene. A major contributing factor is the lack of large PAHs in the RMG model. In the experiment, PAHs with three or more rings accounted for 28% of product carbons at 1373 K, with 12% in PAHs not even included in the RMG model. Additionally, the C:H ratio of the experimentally measured product composition at 1373 K is approximately 1:2.78, not the 1:1 ratio of the feed, which suggests that some carbon-rich products (*i.e.*, soot or coke) were formed which were not quantified. Since the RMG model stops at pyrene, there are no further consumption channels for acetylene, leading to the over-prediction. In contrast, at 1073 K, large PAHs only make up 2.7% of the product carbons, and the experimental C:H ratio is 1:1.03, suggesting minimal soot formation.

Figures 4 and 5 show the top 10 pathways for acetylene consumption at 1373 K and 1073 K, respectively, predicted by our model. An overall observation is that acetylene consumption is not highly dominated by a single channel, but is instead relatively spread out. At 1373 K, the top 10 pathways only account for 69% of total acetylene consumption, and the top 60 pathways have to be considered before reaching 99%. We see that almost all of the top pathways involve radical addition to acetylene, the exceptions being isomerization to vinylidene and vinylidene addition. Additionally, most of these pathways are well-skipping pathways in pressure dependent networks, indicating the importance of considering pressure-dependence for this system.

Notably, acetylene dimerization to either vinylacetylene (R1) or diacetylene (R2) do not appear in the top 10 acetylene consumption pathways according to the RMG model. This is in stark contrast to the other models which were evaluated.

$$C{\equiv}C + C{\equiv}C \rightleftharpoons C{\equiv}C{-}C{=}C \tag{R1}$$

$$C{\equiv}C + C{\equiv}C \rightleftharpoons C{\equiv}C{-}C{\equiv}C + H_2 \tag{R2}$$

The vinylacetylene formation reaction (R1) is present in all four models, with vast differences in the rate parameters, as shown in Figure 6. The RMG model uses the pressure dependent rate coefficient calculated by Zádor *et al.* for the C_4H_4 potential energy surface.[35] The Slavinskaya model cites Melius *et al.*,[51] although there is approximately a factor of 2 discrepancy in the activation energy. The Norinaga and Tao models have very similar rate coefficients, for which Norinaga cited Dúran *et al.*[52] and Tao cited Saggase *et al.*[53]

The diacetylene formation reaction (R2) was intentionally removed from the Slavinskaya model, because they noted that it was the sum of two reactions proceeding via $H_2CCCCH + H$. R2 is included in the other models, with the RMG model using the pressure-dependent rate coefficient computed by Zádor *et al.* The Norinaga and Tao models have identical rate coefficients for this reaction, taken from Fournet *et al.*[54] There is a notable difference between the two literature values for this rate coefficient.

For the Zádor rate coefficients, the total rate considering both entrance channel I ($C{\equiv}C + C{\equiv}C$) and III ($C{\equiv}C + :C{=}CH_2$) is shown in addition to the rate from I only. The rate from III was multiplied by the

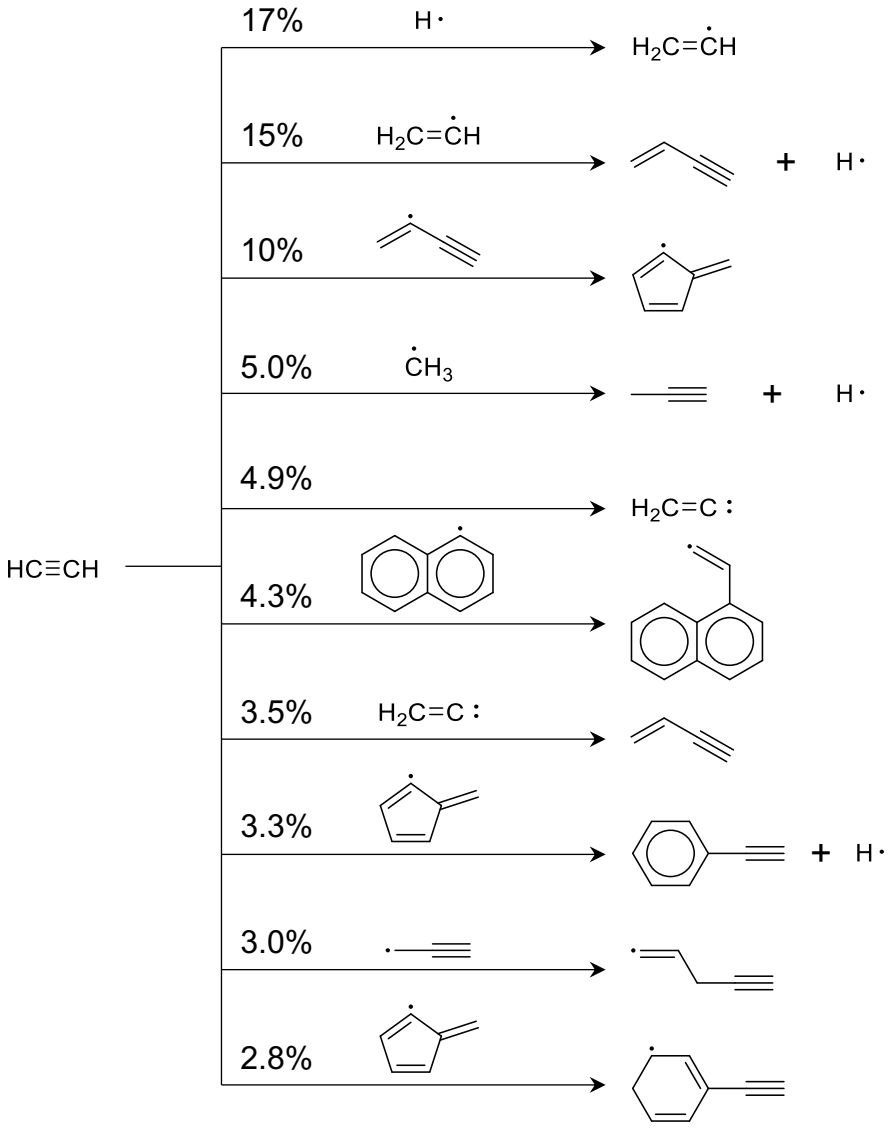

Figure 4: Top 10 consumption pathways of acetylene at conditions of ref. [49], 1373 K set point. Values indicate integrated molar flux through each pathway as a percentage of total acetylene flux.

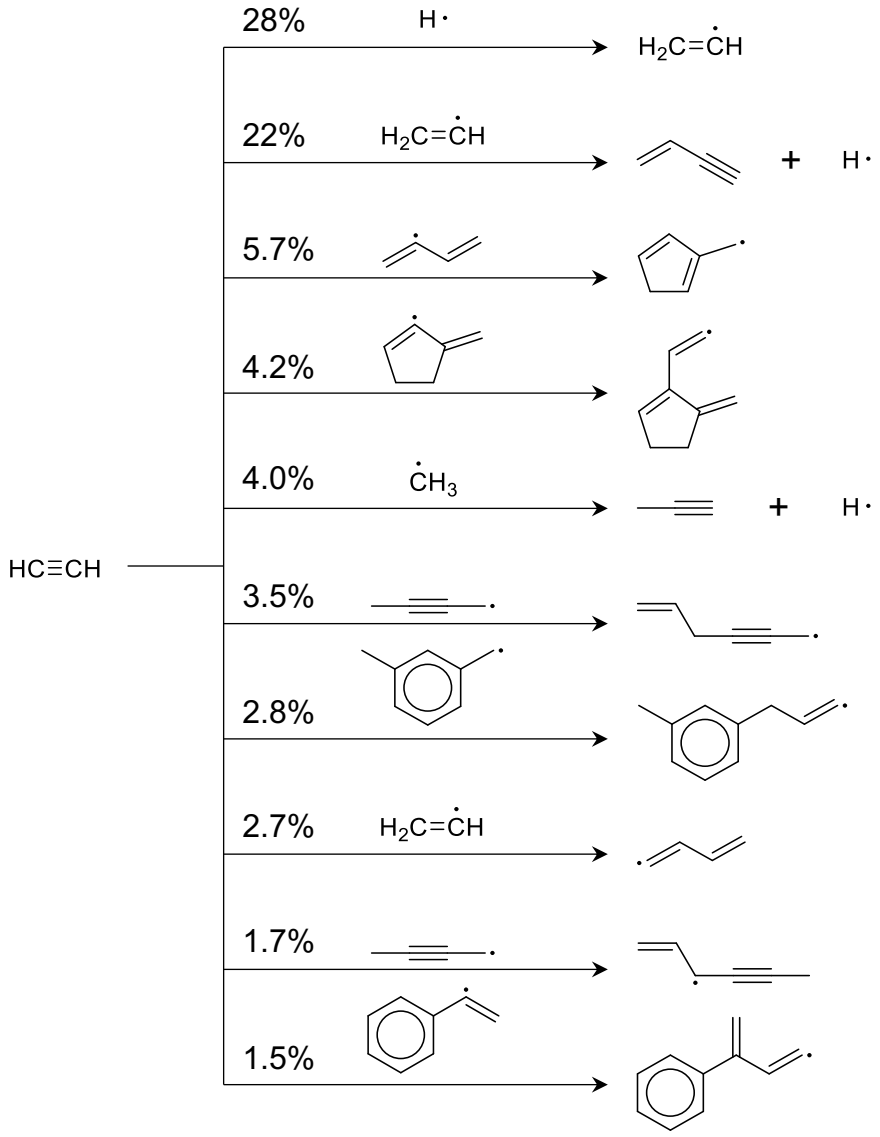

Figure 5: Top 10 consumption pathways of acetylene at conditions of ref. [49], 1073 K set point. Values indicate integrated molar flux through each pathway as a percentage of total acetylene flux.

[:C=CH_2]/[C≡C] equilibrium constant before summing. For both reactions, the Zádor rate coefficients are slower in comparison to the experimental data. However, it is important to keep in mind that the experimental measurements are not direct measurements of the reactions of interest. In particular, the experiments which measured acetylene consumption would include all product routes. The agreement between the experimental data and the Norinaga rate coefficient for R1 is expected given that Dúran *et al.* fitted the rate coefficient to the experimental data.

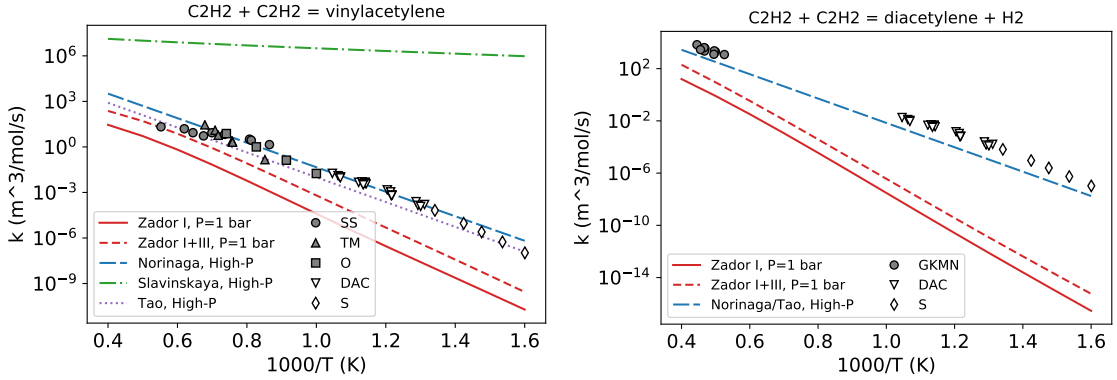

Figure 6: Comparison of rate coefficients for formation of vinylacetylene (left) and diacetylene (right) via acetylene dimerization used in different models. Points indicate experimental values and are labeled with first letters of the authors' last names.[55, 56, 57, 58, 59, 60] Marker fill color indicates measurement of product formation (gray) vs. acetylene consumption (white).

With the calculated rate coefficients by Zádor *et al.*, it seems that direct formation of vinylacetylene or diacetylene (realistically through a chemically-activated reaction) is not a particularly significant pathway at these conditions.

3.2. Role of acetone

As mentioned previously, the inclusion of the acetone impurity in the feed in the model significantly affected both acetylene conversion and product distributions. Acetone primarily decomposes into ketene or carbon monoxide, releasing up to two methyl radicals in the process, as shown in Figure 7. Ketene is favored at lower temperatures, while carbon monoxide is favored at higher temperatures, leading to increased formation of methyl radicals. The methyl radicals then contribute significantly to the formation of odd-carbon species. Methyl addition to acetylene can proceed through a well-skipping pathway to form propyne or allene. These C_3 species can then form propargyl radicals, which greatly simplify the process of reaching C_5 (*e.g.*, cyclopentadiene), C_7 (*e.g.*, toluene), and C_9 (*e.g.*, indene). Simulations with the RMG model assuming pure acetylene as the feed results in substantial under-prediction of all of these odd-carbon species.

3.3. Small molecule products

Low molecular weight products which were reported in the experiment include H_2, CH_4, C_2H_4, allene, and propyne. Overall, the RMG model predictions match the experimental data very well for these species.

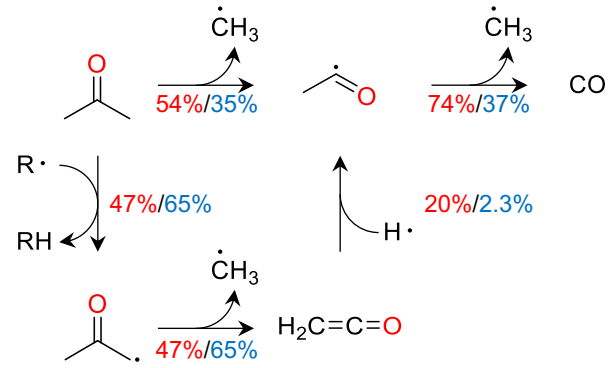

Figure 7: Acetone decomposition pathways. Values indicate integrated molar flux through each pathway as a percentage of total acetone flux. First value in red indicates flux at 1373 K and second value in blue indicates flux at 1073 K. Pathways with values less than 1% are omitted.

The most significant deviation is for hydrogen, which is under-predicted by about a factor of two at low temperatures and a factor of three at higher temperatures. This discrepancy is likely also related to the under-prediction of large PAH formation in the RMG model, since conversion of acetylene to carbon-rich PAHs results in elimination of hydrogen.

Hydrogen, methane, and ethylene are all formed via hydrogen abstraction, primarily from molecules like propyne, vinylacetylene, cyclopentadiene, indene, and acetone to form resonance-stabilized radicals (RSRs), *e.g.*, propargyl, etc. These reactions (*e.g.*, $H\cdot + C_3H_4 \rightleftharpoons H_2 + C_3H_3$) are key chain-propagation steps to formation of larger compounds, as the RSRs then add to acetylene or vinylacetylene to continue molecular weight growth, with the exception of 1-methylvinoxy which primarily breaks apart into ketene and a methyl radical as mentioned above.

Propyne and allene, on the other hand, are primarily formed via chemically-activated pathways, as shown in Figure 8. The most significant pathway is methyl addition to acetylene to form propyne, which can then isomerize to form allene.

Vinylacetylene is primarily formed via chemically activated pathways, the primary pathway being vinyl addition to acetylene, and the secondary pathway being vinylidene addition to acetylene, as shown in Figure 9. The vinylidene pathway becomes more significant at higher temperatures, due to higher flux of acetylene isomerization to vinylidene. The vinyl addition pathway can also proceed via C_4H_5 radical intermediates, which play important roles in aromatic ring formation.[61] At lower temperatures, formation of both C_4H_5 radicals increases, and the net flux of H-elimination from i-C_4H_5 goes in the reverse direction, consuming vinylacetylene instead. Diacetylene is formed via H-elimination or disproportionation from C_4H_3 radicals, which are mostly formed via hydrogen abstraction from vinylacetylene, with a small contribution from C_2H addition to acetylene. As mentioned previously, dimerization of acetylene was not found to contribute significantly to either vinylacetylene or diacetylene at these conditions.

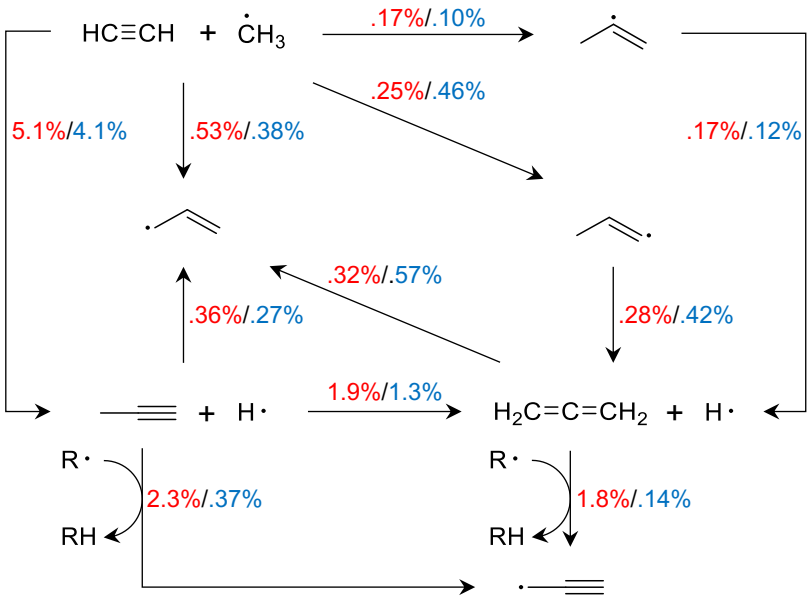

Figure 8: Main pathways to C_3 species. Values indicate integrated molar flux through each pathway as a percentage of total acetylene flux. First value in red indicates flux at 1373 K and second value in blue indicates flux at 1073 K set point conditions of ref. [49]. Pathways with values less than 0.1% are omitted.

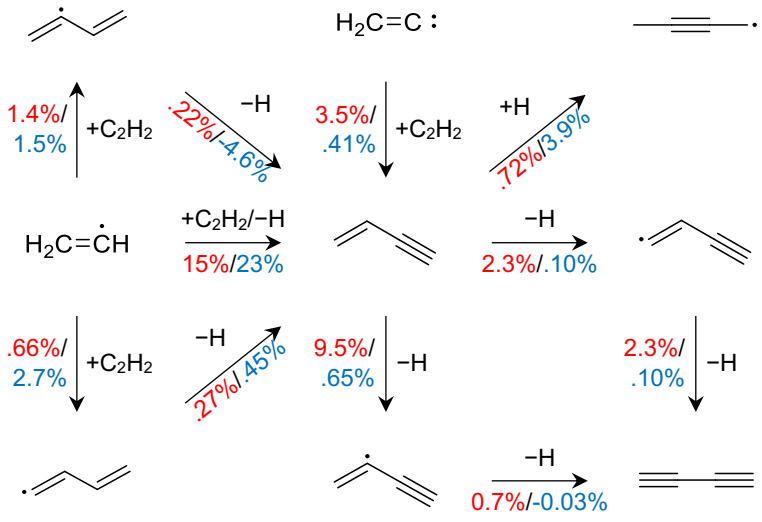

Figure 9: Main pathways to C_4 species. Values indicate integrated molar flux through each pathway as a percentage of total acetylene flux. First value in red indicates flux at 1373 K and second value in blue indicates flux at 1073 K set point conditions of ref. [49]. Pathways with values less than 0.1% are omitted. −H can include H-elimination, H-abstraction, or disproportionation.

3.4. One- and two-ring aromatic species

Looking at single ring aromatics in Figure 3, benzene and toluene are reasonably predicted, but styrene diverges from experiment at low temperatures and phenylacetylene diverges at high temperatures. From the reaction path analysis for benzene, shown in Figure 10, we see that the primary pathway for benzene formation is via methylcyclopentadienyl, which is generated through multiple C_4 + C_2H_2 pathways, all involving many isomerization and H-shift steps. A secondary pathway is via cyclohexadienyl radical, which is formed by 1-butadienyl addition to acetylene. Phenyl addition to benzene is the primary pathway leading to biphenyl formation, with phenyl recombination flux being the second pathway with a thousand times smaller flux.

The RMG model predicts styrene well at high temperatures, but begins to under-predict its formation below 1273 K. Interestingly, this is in contrast with the other literature models which tend to over-predict styrene formation. For phenylacetylene, the RMG model over-predicts formation at high temperatures, which is similar in behavior to both the Tao and Slavinskaya models. In the RMG model, the fulvenyl and phenylvinyl radicals are the primary precursors to both phenylacetylene and styrene. From phenylvinyl, H-elimination to phenylacetylene is much more favored than H-abstraction to form styrene. Vinyl addition to benzene can also lead to styrene, but was found to have negligible flux, likely because it breaks the aromaticity of the benzene ring.

Both toluene and indene are well predicted by the RMG model. Since these are both odd-carbon species, propargyl plays a major role in their formation. The primary route to toluene is via propargyl addition to vinylacetylene, which proceeds via a well-skipping route to directly form a benzyl radical, as shown in Figure 11. Alternatively, benzyl can also be formed by cyclopentadienyl (CPDyl) radical addition to acetylene followed by a few isomerization steps. However, toluene is actually a very small consumption pathway of benzyl, which at the conditions of ref. [49] instead prefers to add another acetylene and ring-close to form indene. The importance of propargyl in these pathways to toluene and indene offers a clear explanation for the low prediction of these species when acetone is not included in the initial composition.

Naphthalene is also predicted reasonably well by the RMG model, although it is over-predicted by about an order of magnitude at 1073 K. Naphthalene can be formed by many different paths, which are shown in Figure 12. The most significant pathway is via cyclopentadienyl recombination, which involves multiple isomerizations and two H-loss steps, which has been previously explored in detail and is included in the RMG database.[62] HACA growth also contributes to naphthalene formation, starting from three different styrene radicals. The most significant HACA route starts from the 1-phenylvinyl radical, which can ring-close to form methylindenyl radical, which can then isomerize and undergo H-loss to naphthalene. The other two routes follow the Bittner-Howard and Modified-Frenklach pathways. The final pathway is via vinyl addition to phenylacetylene, which proceeds through many of the same intermediates as the other two pathways before the final H-elimination step to form naphthalene.

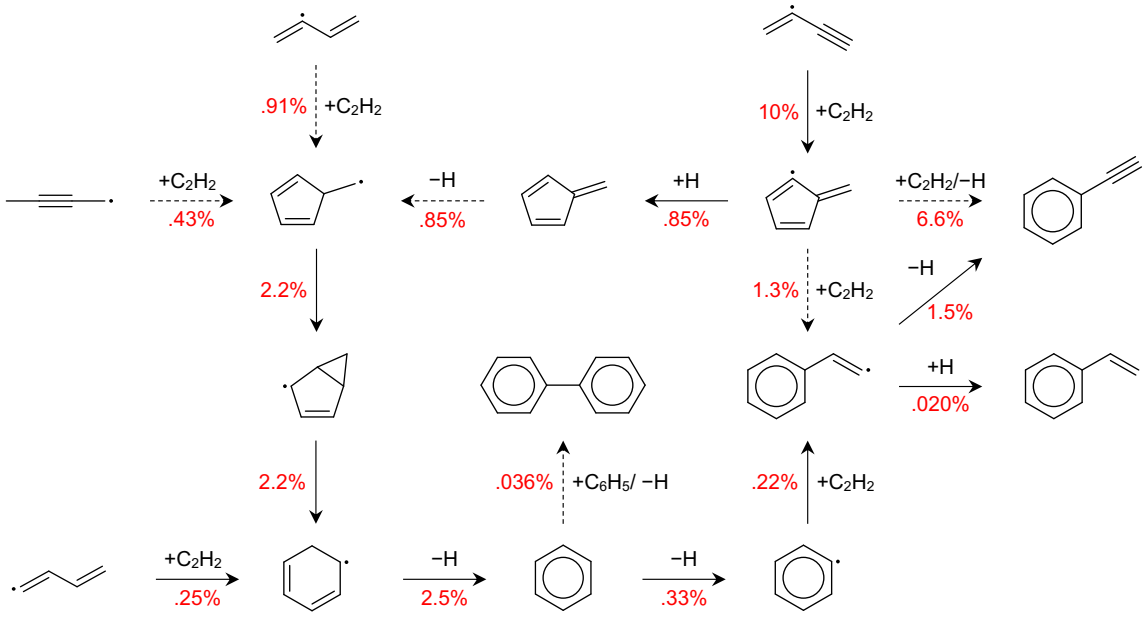

Figure 10: Main pathways to mono-aromatic species and biphenyl at 1373 K, conditions of [49]. Values indicate integrated molar flux through each pathway as a percentage of total acetylene flux. Pathways with values less than 0.01% are omitted. Dashed lines represent a combination of multiple reaction steps. ±H can include H-elimination, H-abstraction, disproportionation, or recombination.

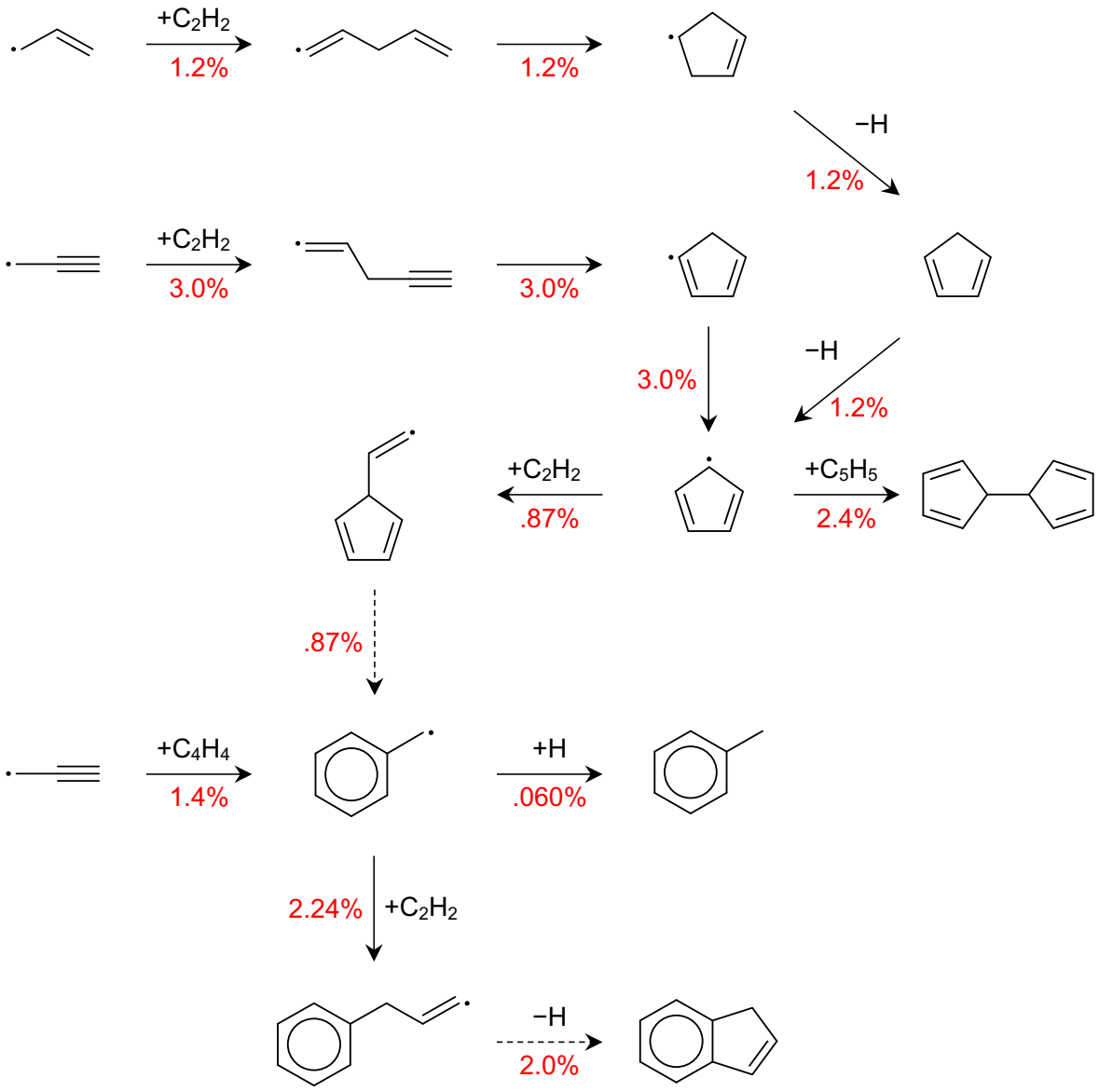

Figure 11: Main pathways to toluene and indene at 1373 K, conditions of [49]. Values indicate integrated molar flux through each pathway as a percentage of total acetylene flux. Pathways with values less than 0.01% are omitted. Dashed lines represent a combination of multiple reaction steps. ±H can include H-elimination, H-abstraction, disproportionation, or recombination.

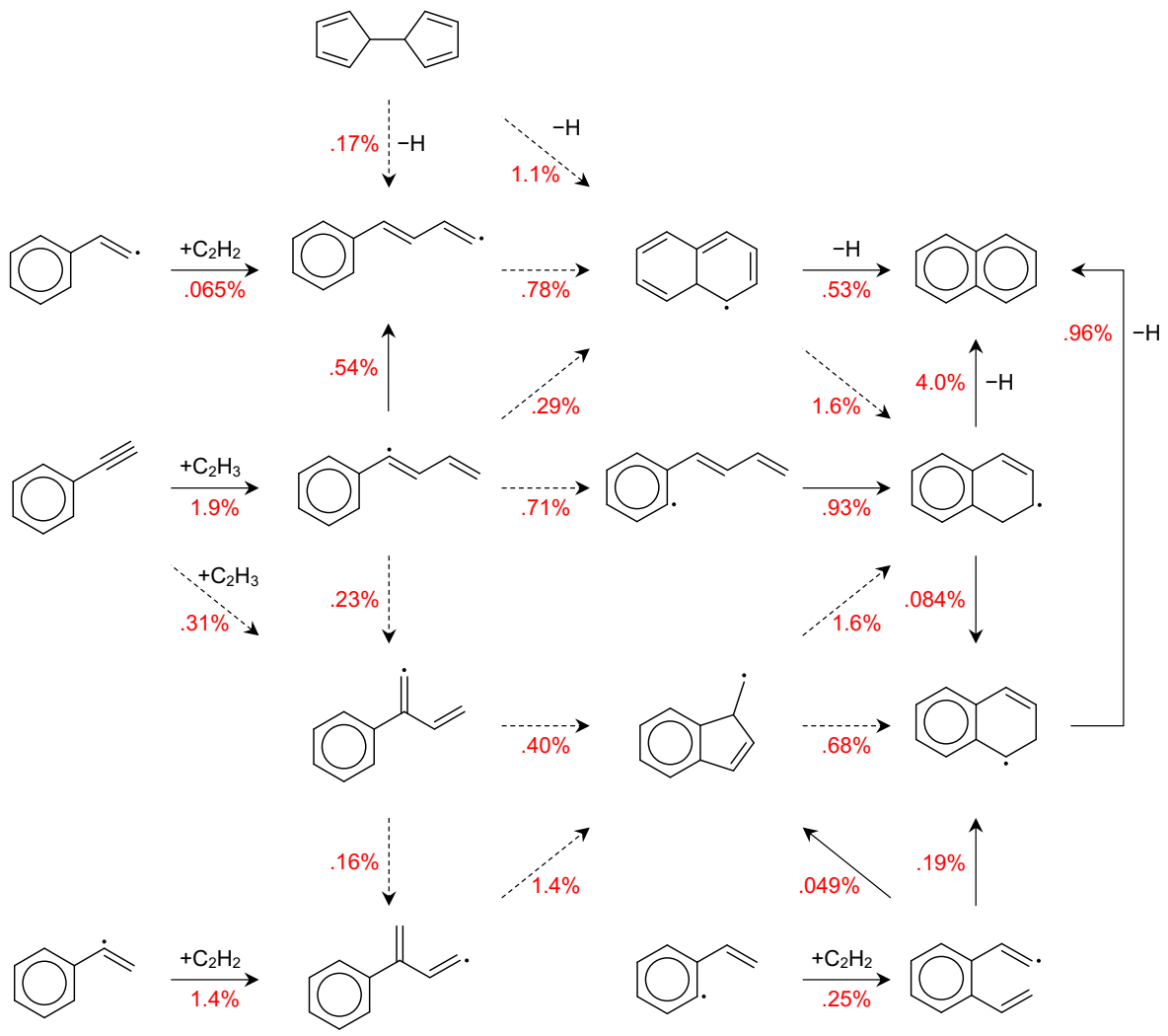

Figure 12: Main pathways to naphthalene at 1373 K, conditions of [49]. Values indicate integrated molar flux through each pathway as a percentage of total acetylene flux. Pathways with values less than 0.01% are omitted. Dashed lines represent a combination of multiple reaction steps. ±H can include H-elimination, H-abstraction, disproportionation, or recombination.

3.5. Three- and four-ring aromatic species

While the acenaphthylene prediction by the RMG model matches reasonably with experiment, once we get to three ring aromatics, we see significant under-prediction by the model. In short, this is due to the limited number of PAH formation pathways which are included in this RMG model. As previously mentioned, a number of pathways for which accurate quantum chemistry data were available were included as kinetics libraries for this model. The RMG simulation was not able to fully explore additional reaction pathways beyond those due to computational limitations of the RMG algorithm in handling such complex chemistry.

At 1373 K, the amount of these three- and four-ring PAHs predicted by the RMG model comes fairly close to matching the experimental measurements, within about a factor of five or better. All of the pathways to these large PAHs fall under the HACA scheme (Figure 13). The main precursor to three-ring aromatics is the naphthalen-1-yl radical, formed either via H-abstraction from naphthalene or the Frenklach pathway for HACA growth from phenylacetylene, which directly forms naphthalen-1-yl without passing through naphthalene. Following addition of acetylene, the most favorable route to acenaphthylene involves an H-shift from the 8-position on the ring to the vinyl group. The ring-closing pathway following the H-shift goes through a stable benzylic intermediate and accounts for about 80% of acenaphthylene formation. The remainder is mostly from the slower, direct ring-closing route which involves disrupting the aromaticity of the ring.

The other major precursor to three-ring aromatics is the naphthalen-2-yl radical, which exclusively forms via H-abstraction. A small fraction undergoes H-shift to naphthalen-1-yl, while the majority adds to acetylene. The 2-naphthalen-2-ylvinyl radical can then go through one of four pathways. The highest-flux pathway is a recently elucidated mechanism involving an H-shift from the 1-position on the ring to the vinyl side-chain forming 2-vinylnaphthalen-1-yl, followed by isomerization to the 2-naphthalen-1-ylvinyl radical via a three-member ring intermediate, which proceeds to form acenaphthylene.[63] A small fraction of the 2-vinylnaphthalen-1-yl radical continues along the Modified-Frenklach pathway via a second acetylene addition to form phenanthrene. The second most significant pathway involves H-elimination to form 2-ethynylnaphthalene, following the Frenklach pathway to form anthracene or phenanthrene in about a 3:2 ratio. The third pathway follows the Bittner-Howard HACA scheme with a second acetylene addition, followed by ring-closing and H-elimination to phenanthrene or anthracene in about a 3:1 ratio. The final pathway is H-shift to the 3-position on the ring, following the Modified-Frenklach pathway to form anthracene. Although reactions for the naphthalenyl + vinylacetylene pathway to phenanthrene and anthracene were included in the model, almost no flux passed through the pathway despite the relative abundance of vinylacetylene.

Finally, biphenyl provides a minor route to phenanthrene, via a single HACA step which closes one of the bay sites in biphenyl. An analogous pathway closes the bay site in phenanthrene to form pyrene. Even though this is the only reaction path to pyrene included in the RMG model, it does lead to a substantial amount of pyrene formation. If phenanthrene formation were to increase (*e.g.*, by adding more pathways

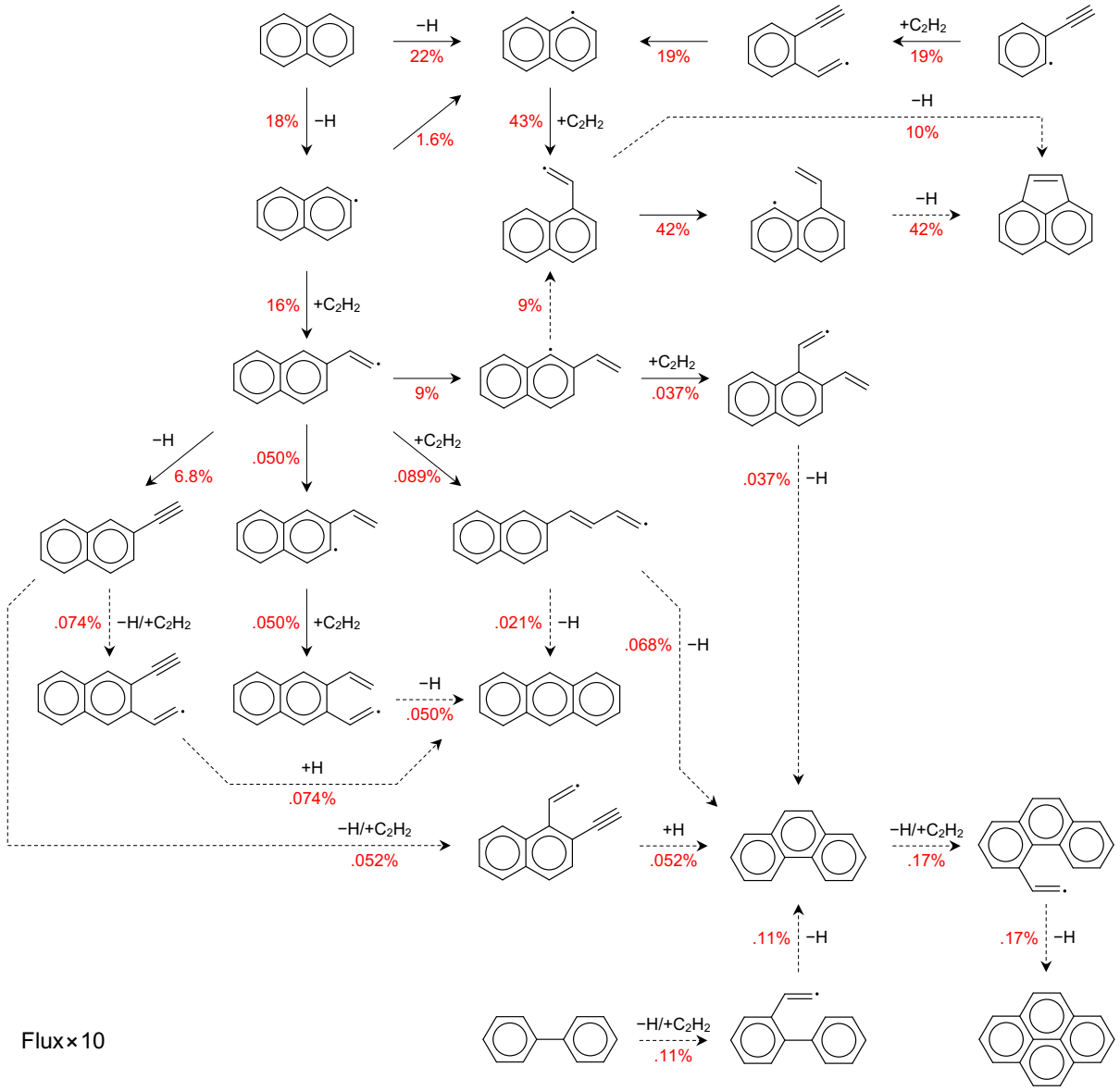

Figure 13: Main pathways to three and four ring aromatic species at 1373 K, conditions of [49]. Values indicate integrated molar flux through each pathway as a percentage of total acetylene flux, multiplied by 10. Pathways with values less than 0.001% are omitted. Dashed lines represent a combination of multiple reaction steps. ±H can include H-elimination, H-abstraction, disproportionation, or recombination.

or improving precursor concentrations), it is likely that this pathway would be sufficient to explain pyrene formation at the high end of the temperature range.

3.6. Sensitivity analysis

Sensitivity analysis was also performed for 12 selected species, including aromatic species of interest and other species for which the model predictions deviated significantly from the experimental measurements: acetylene, vinylacetylene, benzene, toluene, phenylacetylene, styrene, indene, naphthalene, acenaphthylene, anthracene, phenanthrene, and pyrene. The top rate and thermochemical parameters which affect each species' mole fractions are shown in Figures S4 to S15 in the supporting information.

There was substantial commonality among the most sensitive rate coefficients and thermochemical parameters. Taking the five most sensitive parameters of each type for the 12 species, there were only 24 unique rate coefficients and 19 unique species thermochemistry, out of a potential total of 120 rate and thermochemistry parameters.

The two reactions with the most appearances were $C_2H_2 + C_2H_3 \rightleftharpoons C_4H_4 + H$ and $C_2H_2 + \text{i-}C_4H_3 \rightleftharpoons C_6H_5$ (fulven-1-yl). In the current model, these two reactions are important steps in the formation of the first aromatic ring, as shown in Figure 10. The rates for both of these reactions were estimated by the pressure-dependence algorithm in RMG, which calculates pressure-dependent rate coefficients from high-pressure-limit rates for elementary steps in the network. Out of the 24 rate coefficients identified as being important, 16 were exact matches to calculated values, five were pressure-dependent RMG estimates, and three were high-pressure-limit RMG estimates.

The two species enthalpies with the most appearances were acetylene and i-C_4H_3. The enthalpy of acetylene was the most sensitive thermochemical parameter affecting the product yields for all the species except toluene, where it was the third most sensitive. This is not unexpected, given that it serves as the main building block in forming all of these species. Out of the 19 species which were identified as most important, only fulven-1-yl was estimated via group additivity, while the remainder were obtained from libraries based on quantum calculations. Ten of the values are from the new CBS-QB3 aromatics thermochemistry library created in this work.

This analysis shows that the key products of interest are sensitive to a handful of rate and thermochemistry parameters. Most of these values are already sourced from reliable library data obtained from quantum chemistry calculations. However, the model could be further improved by replacing the remaining estimates with calculations, especially for the eight RMG estimated rate coefficients identified in the analysis, which are marked in Figures S1 to S12.

4. Conclusions

In this work, we have demonstrated the ability of RMG to automatically generate a mechanism to predict PAH formation in acetylene pyrolysis. Kinetics and thermochemistry data for key PAH formation pathways

and acetylene initiation pathways have been calculated using Arkane and added to the RMG database. Using the newly added data, a detailed chemical mechanism with 1594 species and 8924 reactions was generated using RMG. Importantly, no manual adjustment or optimization of thermochemical and kinetic parameters was performed following model generation. The unadjusted model predictions agree well with experimental flow reactor data, particularly for small molecule products and one- to two-ring aromatics. Acetylene consumption is under-predicted, which is most likely linked to the under-prediction of three- and four-ring aromatic species.

Acetylene consumption was found to be relatively spread out across many different pathways, in contrast to dominance of direct dimerization to vinylacetylene or diacetylene which was characteristic of previous literature models. The impurity acetone present in the experiments was found to play an important role in the formation of odd-carbon species, from methane up to indene, despite its low initial concentration. Because the Slavinskaya and Tao models did not include acetone, they tended to under-predict the formation of these species. These results provide some insight into the broader role of acetone, beyond only acting as a radical initiator.

For PAHs, the majority of formation pathways captured by the RMG model can be classified as part of the HACA mechanism. The main exception is cyclopentadienyl recombination, which contributed significantly to the formation of naphthalene. The three main types of HACA pathways (Bittner-Howard, Modified-Frenklach, and Frenklach) were all observed to contribute to formation of naphthalene from benzene and phenanthrene/anthracene from naphthalene. The under-prediction of these large PAHs suggests that the included pathways are not sufficient to explain their formation and that other pathways may be missing. Testing the PAH sub-mechanism in a system like ethylene pyrolysis could provide further insight by removing much of the uncertainty associated with acetylene initiation and acetone.

This work represents an important milestone for the RMG software in automatically generating a mechanism predicting up to pyrene. However, there are still improvements which can be made to both the software and the chemical mechanism. Notably, generation of PAH formation models is still computationally challenging due to the sheer number of potential species and reactions which RMG evaluates. Additionally, highly-strained species tend to be over-represented in the RMG model due to poor thermochemistry estimates. On the chemistry side, accurate thermochemical and kinetic data for more species and pathways is important for improving the accuracy of the models, which rely heavily on the accuracy of *ab initio* calculations and estimation methods. We think the analysis presented in this work can help guide future work to improve these model parameters.

5. Acknowledgements

We gratefully acknowledge Professor Alexander Mebel for providing us with electronic structure data to aid our calculations.

Financial support from SABIC is also gratefully acknowledged. Agnes Jocher acknowledges financial support from the DFG Research Fellowship under JO 1526/1-1.

6. Supporting Information

Additional supporting information is available:

- Sensitivity analysis of key observables to rate coefficients and thermochemical parameters
- Acetylene mechanism in CHEMKIN format + RMG species dictionary
- RMG input file used to generate base acetylene mechanism
- Calculated aromatic thermochemistry data in CHEMKIN format + RMG species dictionary
- PAH sub-mechanism in CHEMKIN format + RMG species dictionary

References

1. Richter H, Howard JB. Formation of polycyclic aromatic hydrocarbons and their growth to soot–a review of chemical reaction pathways. *Prog Energy Combust Sci* 2000;26(4-6):565–608. URL: http://www.sciencedirect.com/science/article/pii/S0360128500000095. doi:10.1016/S0360-1285(00)00009-5.

2. Léger A, D'Hendecourt L, Boccara N. Polycyclic Aromatic Hydrocarbons and Astrophysics. NATO ASI Series, Series C: Mathematical and Physical Sciences, 1389-2185: 191; Dordrecht : Springer Netherlands, 1986.; 1986. ISBN 9789400947764. URL: https://search.ebscohost.com/login.aspx?direct=true{&}db=cat00916a{&}AN=mit.002279930{&}site=eds-live{&}scope=sitehttps://library.mit.edu/F/?func=service-sfx{&}doc{_}number=002279930{&}line{_}number=0000{&}service{_}type=RECORD.

3. Frenklach M, Feigelson ED. Formation of Polycyclic Aromatic Hydrocarbons in Circumstellar Envelopes. *Astrophys J* 1989;341:372. URL: https://ui.adsabs.harvard.edu/abs/1989ApJ...341..372F. doi:10.1086/167501.

4. Kim KH, Jahan SA, Kabir E, Brown RJ. A review of airborne polycyclic aromatic hydrocarbons (PAHs) and their human health effects. *Environ Int* 2013;60:71–80. URL: https://www.sciencedirect.com/science/article/pii/S0160412013001633. doi:10.1016/J.ENVINT.2013.07.019.

5. Frenklach M. Reaction mechanism of soot formation in flames. *Phys Chem Chem Phys* 2002;4(11):2028–37. doi:10.1039/b110045a.

6. Frenklach M, Clary DW, Gardiner WC, Stein SE. Detailed kinetic modeling of soot formation in shock-tube pyrolysis of acetylene. *Symp Combust* 1985;20(1):887–901. URL: http://www.sciencedirect.com/science/article/pii/S0082078485805786. doi:10.1016/S0082-0784(85)80578-6.

7. Westmoreland PR, Dean AM, Howard JB, Longwell JP. Forming benzene in flames by chemically activated isomerization. *J Phys Chem* 1989;93(25):8171–80. URL: http://dx.doi.org/10.1021/j100362a008. doi:10.1021/j100362a008.

8. Wang H, Frenklach M. Calculations of Rate Coefficients for the Chemically Activated Reactions of Acetylene with Vinylic and Aromatic Radicals. *J Phys Chem* 1994;98(44):11465–89. URL: http://dx.doi.org/10.1021/j100095a033. doi:10.1021/j100095a033.

9. Miller JA, Klippenstein SJ. The Recombination of Propargyl Radicals and Other Reactions on a C6H6 Potential. *J Phys Chem A* 2003;107(39):7783–99. URL: http://dx.doi.org/10.1021/jp030375h. doi:10.1021/jp030375h.

10. Marinov NM, Castaldi MJ, Melius CF, Tsang W. Aromatic and Polycyclic Aromatic Hydrocarbon Formation in a Premixed Propane Flame. *Combust Sci Technol* 1997;128(1-6):295–342. URL: http://www.tandfonline.com/doi/abs/10.1080/00102209708935714. doi:10.1080/00102209708935714.

11. Melius CF, Colvin ME, Marinov NM, Pitz WJ, Senkan SM. Reaction mechanisms in aromatic hydrocarbon formation involving the C5H5 cyclopentadienyl moiety. *Symp Combust* 1996;26(1):685–92. URL: http://www.sciencedirect.com/science/article/pii/S0082078496802761. doi:10.1016/S0082-0784(96)80276-1.

12. Moskaleva LV, Mebel AM, Lin MC. The CH3+C5H5 reaction: A potential source of benzene at high temperatures. *Symp Combust* 1996;26(1):521–6. URL: http://www.sciencedirect.com/science/article/pii/S0082078496802554. doi:10.1016/S0082-0784(96)80255-4.

13. Sharma S, Green WH. Computed rate coefficients and product yields for c-C5H5 + CH3 –> products. *J Phys Chem A* 2009;113(31):8871–82. URL: http://dx.doi.org/10.1021/jp900679t. doi:10.1021/jp900679t.

14. Mebel AM, Landera A, Kaiser RI. Formation Mechanisms of Naphthalene and Indene: From the Interstellar Medium to Combustion Flames. *J Phys Chem A* 2017;121(5):901–26. doi:10.1021/acs.jpca.6b09735.

15. Bittner JD, Howard JB. Composition profiles and reaction mechanisms in a near-sooting premixed benzene/oxygen/argon flame. *Symp Combust* 1981;18(1):1105–16. URL: http://www.sciencedirect.com/science/article/pii/S0082078481801154. doi:10.1016/S0082-0784(81)80115-4.

16. Mebel AM, Georgievskii Y, Jasper AW, Klippenstein SJ. Temperature- and pressure-dependent rate coefficients for the HACA pathways from benzene to naphthalene. *Proc Combust Inst* 2017;36(1):919–26. URL: https://www.sciencedirect.com/science/article/pii/S1540748916302693. doi:10.1016/J.PROCI.2016.07.013.

17. Kislov VV, Sadovnikov AI, Mebel AM. Formation mechanism of polycyclic aromatic hydrocarbons beyond the second aromatic ring. *J Phys Chem A* 2013;117(23):4794–816. URL: http://dx.doi.org/10.1021/jp402481y. doi:10.1021/jp402481y.

18. Frenklach M, Singh RI, Mebel AM. On the low-temperature limit of HACA. *Proc Combust Inst* 2019;37(1):969–76. URL: https://doi.org/10.1016/j.proci.2018.05.068. doi:10.1016/j.proci.2018.05.068.

19. Liu P, Li Z, Bennett A, Lin H, Sarathy SM, Roberts WL. The site effect on PAHs formation in HACA-based mass growth process. *Combust Flame* 2019;199:54–68. URL: https://linkinghub.elsevier.com/retrieve/pii/S0010218018304371. doi:10.1016/j.combustflame.2018.10.010.

20. Yang T, Kaiser RI, Troy TP, Xu B, Kostko O, Ahmed M, Mebel AM, Zagidullin MV, Azyazov VN. HACA's Heritage: A Free-Radical Pathway to Phenanthrene in Circumstellar Envelopes of Asymptotic Giant Branch Stars. *Angew Chemie Int Ed* 2017;56(16):4515–9. URL: http://doi.wiley.com/10.1002/anie.201701259. doi:10.1002/anie.201701259.

21. Zhao L, Kaiser RI, Xu B, Ablikim U, Ahmed M, Joshi D, Veber G, Fischer FR, Mebel AM. Pyrene synthesis in circumstellar envelopes and its role in the formation of 2D nanostructures. *Nat Astron* 2018;2(5):413–9. URL: http://www.nature.com/articles/s41550-018-0399-y. doi:10.1038/s41550-018-0399-y.

22. Zhao L, Kaiser RI, Xu B, Ablikim U, Ahmed M, Zagidullin MV, Azyazov VN, Howlader AH, Wnuk SF, Mebel AM. VUV Photoionization Study of the Formation of the Simplest Polycyclic Aromatic Hydrocarbon: Naphthalene (C10H8). *J Phys Chem Lett* 2018;9(10):2620–6. doi:10.1021/acs.jpclett.8b01020.

23. Zhao L, Kaiser RI, Xu B, Ablikim U, Ahmed M, Evseev MM, Bashkirov EK, Azyazov VN, Mebel AM. Low-temperature formation of polycyclic aromatic hydrocarbons in Titan's atmosphere. *Nat Astron* 2018;2(12):973–9. URL: https://www.nature.com/articles/s41550-018-0585-y. doi:10.1038/s41550-018-0585-y.

24. Fahr A, Stein SE. Reactions of vinyl and phenyl radicals with ethyne, ethene and benzene. *Symposium (International) on Combustion* 1989;22(1):1023–9. URL: https://www.sciencedirect.com/science/article/pii/S0082078489801122. doi:10.1016/S0082-0784(89)80112-2.

25. Park J, Burova S, Rodgers AS, Lin MC. Experimental and Theoretical Studies of the C6H5 + C6H6 Reaction. *J Phys Chem A* 1999;103(45):9036–41. URL: https://pubs.acs.org/doi/abs/10.1021/jp9920592. doi:10.1021/JP9920592.

26. Comandini A, Brezinsky K. Theoretical Study of the Formation of Naphthalene from the Radical/π-Bond Addition between Single-Ring Aromatic Hydrocarbons. *J Phys Chem A* 2011;115(22):5547–59. URL: http://pubs.acs.org/doi/abs/10.1021/jp200201c. doi:10.1021/jp200201c.

27. Comandini A, Abid S, Chaumeix N. Polycyclic Aromatic Hydrocarbon Growth by Diradical Cycloaddition/Fragmentation. *J Phys Chem A* 2017;121(31):5921–31. URL: http://pubs.acs.org/doi/10.1021/acs.jpca.7b05562. doi:10.1021/acs.jpca.7b05562.

28. Durán RP, Amorebieta VT, Colussi AJ. Is the homogeneous thermal dimerization of acetylene a free-radical chain reaction? Kinetic and thermochemical analysis. *J Phys Chem* 1988;92(3):636–40. URL: https://pubs.acs.org/doi/abs/10.1021/j100314a014. doi:10.1021/j100314a014.

29. Kiefer JH, Von Drasek WA, Von Drasek WA. The mechanism of the homogeneous pyrolysis of acetylene. *Int J Chem Kinet* 1990;22(7):747–86. URL: http://doi.wiley.com/10.1002/kin.550220710. doi:10.1002/kin.550220710.

30. Benson SW. Radical processes in the pyrolysis of acetylene. *Int J Chem Kinet* 1992;24(3):217–37. URL: http://doi.wiley.com/10.1002/kin.550240302. doi:10.1002/kin.550240302.

31. Colket MB, Seery DJ, Palmer HB. The pyrolysis of acetylene initiated by acetone. *Combust Flame* 1989;75(3-4):343–66. URL: https://www.sciencedirect.com/science/article/pii/0010218089900485. doi:10.1016/0010-2180(89)90048-5.

32. Kern R, Xie K, Chen H, Kiefer J. High temperature pyrolyses of acetylene and diacetylene behind reflected shock waves. *Symp Combust* 1991;23(1):69–75. URL: https://www.sciencedirect.com/science/article/pii/S0082078406802432. doi:10.1016/S0082-0784(06)80243-2.

33. Cremer D, Kraka E, Joo H, Stearns JA, Zwier TS. Exploration of the potential energy surface of C4H4 for rearrangement and decomposition reactions of vinylacetylene: A computational study. Part I. *Phys Chem Chem Phys* 2006;8(45):5304. URL: http://xlink.rsc.org/?DOI=b609284e. doi:10.1039/b609284e.

34. Mebel AM, Kislov VV, Kaiser RI. Ab initio/Rice-Ramsperger-Kassel-Marcus study of the singlet C4H4 potential energy surface and of the reactions of C2(XΣg+1) with C4H4(XA1g+1) and C(D1) with C3H4 (allene and methylacetylene). *J Chem Phys* 2006;125(13):133113. URL: http://aip.scitation.org/doi/10.1063/1.2227378. doi:10.1063/1.2227378.

35. Zádor J, Fellows MD, Miller JA. Initiation Reactions in Acetylene Pyrolysis. *J Phys Chem A* 2017;121(22):4203–17. URL: http://pubs.acs.org/doi/10.1021/acs.jpca.7b03040. doi:10.1021/acs.jpca.7b03040.

36. Norinaga K, Deutschmann O. Detailed Kinetic Modeling of Gas-Phase Reactions in the Chemical Vapor Deposition of Carbon from Light Hydrocarbons. *Ind Eng Chem Res* 2007;46(11):3547–57. URL: https://pubs.acs.org/doi/abs/10.1021/ie061207p. doi:10.1021/IE061207P.

37. Slavinskaya NA, Mirzayeva A, Whitside R, Starke J, Abbasi M, Auyelkhankyzy M, Chernov V. A modelling study of acetylene oxidation and pyrolysis. *Combust Flame* 2019;210:25–42. URL: https://www.sciencedirect.com/science/article/pii/S0010218019303876?dgcid=rss{_}sd{_}all{#}bib0031. doi:10.1016/J.COMBUSTFLAME.2019.08.024.

38. Tao H, Wang HY, Ren W, Lin KC. Kinetic mechanism for modeling the temperature effect on PAH formation in pyrolysis of acetylene. *Fuel* 2019;255(January):115796. URL: https://doi.org/10.1016/j.fuel.2019.115796. doi:10.1016/j.fuel.2019.115796.

39. Gao CW, Allen JW, Green WH, West RH. Reaction Mechanism Generator: Automatic construction of chemical kinetic mechanisms. *Comput Phys Commun* 2016;203:212–25. URL: https://linkinghub.elsevier.com/retrieve/pii/S0010465516300285. doi:10.1016/j.cpc.2016.02.013.

40. Chu TC, Buras ZJ, Oßwald P, Liu M, Goldman MJ, Green WH. Modeling of aromatics formation in fuel-rich methane oxy-combustion with an automatically generated pressure-dependent mechanism. *Phys Chem Chem Phys* 2019;21(2):813–32. URL: http://xlink.rsc.org/?DOI=C8CP06097E. doi:10.1039/C8CP06097E.

41. Frisch MJ, Trucks GW, Schlegel HB, Scuseria GE, Robb MA, Cheeseman JR, Scalmani G, Barone V, Petersson GA, Nakatsuji H, Li X, Caricato M, Marenich AV, Bloino J, Janesko BG, Gomperts R, Mennucci B, Hratchian HP, Ortiz JV, Izmaylov AF, Sonnenberg JL, Williams-Young D, Ding F, Lipparini F, Egidi F, Goings J, Peng B, Petrone A, Henderson T, Ranasinghe D, Zakrzewski VG, Gao J, Rega N, Zheng G, Liang W, Hada M, Ehara M, Toyota K, Fukuda R, Hasegawa J, Ishida M, Nakajima T, Honda Y, Kitao O, Nakai H, Vreven T, Throssell K, Montgomery, Jr. JA, Peralta JE, Ogliaro F, Bearpark MJ, Heyd JJ, Brothers EN, Kudin KN, Staroverov VN, Keith TA, Kobayashi R, Normand J, Raghavachari K, Rendell AP, Burant JC, Iyengar SS, Tomasi J, Cossi M, Millam JM, Klene M, Adamo C, Cammi R, Ochterski JW, Martin RL, Morokuma K, Farkas O, Foresman JB, Fox DJ. Gaussian 16, Revision C.01. 2016.

42. Werner HJ, Knowles PJ, Knizia G, Manby FR, Schütz M, Celani P, Györffy W, Kats D, Korona T, Lindh R, Mitrushenkov A, Rauhut G, Shamasundar KR, Adler TB, Amos RD, Bernhardsson A, Berning A, Cooper DL, Deegan MJO, Dobbyn AJ, Eckert F, Goll E, Hampel C, Hesselmann A, Hetzer G, Hrenar

T, Jansen G, Köppl C, Liu Y, Lloyd AW, Mata RA, May AJ, McNicholas SJ, Meyer W, Mura ME, Nicklass A, O'Neill DP, Palmieri P, Peng D, Pflüger K, Pitzer R, Reiher M, Shiozaki T, Stoll H, Stone AJ, Tarroni R, Thorsteinsson T, Wang M. MOLPRO, version 2015.1, a package of ab initio programs. 2015.

43. Grinberg Dana A, RMG Team . Automated Reaction Kinetics and Network Exploration (Arkane). 2020. URL: https://github.com/ReactionmechanismGenerator/RMG-Py.

44. Georgievskii Y, Miller JA, Burke MP, Klippenstein SJ. Reformulation and Solution of the Master Equation for Multiple-Well Chemical Reactions. *J Phys Chem A* 2013;117(46):12146–54. URL: http://pubs.acs.org/doi/10.1021/jp4060704. doi:10.1021/jp4060704.

45. Frisch MJ, Trucks GW, Schlegel HB, Scuseria GE, Robb MA, Cheeseman JR, Scalmani G, Barone V, Petersson GA, Nakatsuji H, Li X, Caricato M, Marenich AV, Bloino J, Janesko BG, Gomperts R, Mennucci B, Hratchian HP, Ortiz JV, Izmaylov AF, Sonnenberg JL, Williams-Young D, Ding F, Lipparini F, Egidi F, Goings J, Peng B, Petrone A, Henderson T, Ranasinghe D, Zakrzewski VG, Gao J, Rega N, Zheng G, Liang W, Hada M, Ehara M, Toyota K, Fukuda R, Hasegawa J, Ishida M, Nakajima T, Honda Y, Kitao O, Nakai H, Vreven T, Throssell K, Montgomery, Jr. JA, Peralta JE, Ogliaro F, Bearpark MJ, Heyd JJ, Brothers EN, Kudin KN, Staroverov VN, Keith TA, Kobayashi R, Normand J, Raghavachari K, Rendell AP, Burant JC, Iyengar SS, Tomasi J, Cossi M, Millam JM, Klene M, Adamo C, Cammi R, Ochterski JW, Martin RL, Morokuma K, Farkas O, Foresman JB, Fox DJ. Gaussian 09, Revision A.02. 2009.

46. Dana AG, Ranasinghe D, Wu OH, Grambow C, Dong X, Johnson M, Goldman M, Liu M, Green WH. ReactionMechanismGenerator/ARC: ARC 1.1.0. 2019. URL: https://zenodo.org/record/3356849. doi:10.5281/ZENODO.3356849.

47. Petersson GA, Malick DK, Wilson WG, Ochterski JW, Montgomery Jr. JA, Frisch MJ. Calibration and comparison of the Gaussian-2, complete basis set, and density functional methods for computational thermochemistry. *J Chem Phys* 1998;109(24):10570. URL: https://aip.scitation.org/doi/10.1063/1.477794. doi:10.1063/1.477794.

48. Liu M, RMG Team . Reaction Mechanism Generator (RMG) v2.4.1. 2019. URL: https://github.com/ReactionMechanismGenerator/RMG-Py/releases/tag/2.4.1.

49. Norinaga K, Janardhanan VM, Deutschmann O. Detailed chemical kinetic modeling of pyrolysis of ethylene, acetylene, and propylene at 1073-1373 K with a plug-flow reactor model. *Int J Chem Kinet* 2008;40(4):199–208. URL: http://doi.wiley.com/10.1002/kin.20302. doi:10.1002/kin.20302.

50. Goodwin DG, Speth RL, Moffat HK, Weber BW. Cantera: An Object-oriented Software Toolkit for

Chemical Kinetics, Thermodynamics, and Transport Processes. 2018. URL: https://www.cantera.org. doi:10.5281/zenodo.1174508.

51. Melius CF, Miller JA, Evleth EM. Unimolecular reaction mechanisms involving C3H4, C4H4, and C6H6 hydrocarbon species. *Symp Combust* 1992;24(1):621–8. URL: https://www.sciencedirect.com/science/article/pii/S0082078406800767. doi:10.1016/S0082-0784(06)80076-7.

52. Durán RP, Amorebieta VT, Colussi AJ. Radical sensitization of acetylene pyrolysis. *Int J Chem Kinet* 1989;21(10):947–58. URL: http://doi.wiley.com/10.1002/kin.550211006. doi:10.1002/kin.550211006.

53. Saggese C, Sánchez NE, Frassoldati A, Cuoci A, Faravelli T, Alzueta MU, Ranzi E. Kinetic Modeling Study of Polycyclic Aromatic Hydrocarbons and Soot Formation in Acetylene Pyrolysis. *Energy & Fuels* 2014;28(2):1489–501. URL: http://pubs.acs.org/doi/abs/10.1021/ef402048q. doi:10.1021/ef402048q.

54. Fournet R, Bauge JC, Battin-Leclerc F. Experimental and modeling of oxidation of acetylene, propyne, allene and 1,3-butadiene. *Int J Chem Kinet* 1999;31(5):361–79. doi:10.1002/(SICI)1097-4601(1999)31:5<361::AID-KIN6>3.0.CO;2-K.

55. Skinner GB, Sokoloski EM. Shock tube experiments on the pyrolysis of acetylene. *Journal of Physical Chemistry* 1961;64(12):1952–3. doi:10.1021/j100841a504.

56. Towell GD, Martin JJ. Kinetic data from nonisothermal experiments: Thermal decomposition of ethane, ethylene, and acetylene. *AIChE Journal* 1961;7(4):693–8. doi:10.1002/aic.690070432.

57. Ogura H. Pyrolysis of Acetylene behind Shock Waves. *Bulletin of the Chemical Society of Japan* 1977;50(5):1044–50. URL: http://www.journal.csj.jp/doi/10.1246/bcsj.50.1044. doi:10.1246/bcsj.50.1044.

58. Durán RP, Amorebieta VT, Colussi AJ. Lack of kinetic hydrogen isotope effect in acetylene pyrolysis. *International Journal of Chemical Kinetics* 1989;21(9):847–58. doi:10.1002/kin.550210909.

59. Silcocks CG. The kinetics of the thermal polymerization of acetylene. *Proceedings of the Royal Society of London Series A Mathematical and Physical Sciences* 1957;242(1231):411–29. URL: https://royalsocietypublishing.org/doi/10.1098/rspa.1957.0185. doi:10.1098/rspa.1957.0185.

60. Gay ID, Kistiakowsky GB, Michael JV, Niki H. Thermal Decomposition of Acetylene in Shock Waves. *The Journal of Chemical Physics* 1965;43(5):1720–6. URL: http://aip.scitation.org/doi/10.1063/1.1696996. doi:10.1063/1.1696996.

61. Smith MC, Liu G, Buras ZJ, Chu TC, Yang J, Green WH. Direct Measurement of Radical-Catalyzed C6H6 Formation from Acetylene and Validation of Theoretical Rate Coefficients for C2H3 + C2H2

and C4H5 + C2H2 Reactions. *The Journal of Physical Chemistry A* 2020;124(14):2871–84. URL: https://pubs.acs.org/doi/10.1021/acs.jpca.0c00558. doi:10.1021/acs.jpca.0c00558.

62. Long AE, Merchant SS, Vandeputte AG, Carstensen HH, Vervust AJ, Marin GB, Van Geem KM, Green WH. Pressure dependent kinetic analysis of pathways to naphthalene from cyclopentadienyl recombination. *Combust Flame* 2018;187:247–56. URL: https://www.sciencedirect.com/science/article/pii/S0010218017303383. doi:10.1016/J.COMBUSTFLAME.2017.09.008.

63. Chu TC, Smith MC, Yang J, Liu M, Green WH. Theoretical Study on the HACA Chemistry of Naphthalenyl Radicals and Acetylene: The formation of C12H8, C14H8, and C14H10 species. *Int J Chem Kinet* 2020;Submitted.

List of Figures

List of Tables